THE INSTITUTE OF MATHEMATICS & ITS APPLICATIONS CONFERENCE SERIES New Series Number 67

MATHEMATICS IN SIGNAL PROCESSING IV

Edited by
J. G. McWHIRTER and
I. K. PROUDLER

McWHIRTER and PROUDLER
MATHEMATICS IN SIGNAL PROCESSING IV
OXFORD

Mathematics in Signal Processing IV

Based on the proceedings of a conference on Mathematics in Signal Processing. Organized by the Institute of Mathematics and its Applications and held at the University of Warwick in December 1996.

Edited by

J. G. McWHIRTER

Head of Signal Processing Group (Senior Fellow)
Defence Evaluation and Research Agency, Malvern

and

I. K. PROUDLER

Defence Evaluation and Research Agency, Malvern

CLARENDON PRESS • OXFORD • 1998

Bayesian Image Estimation from Sparse Raw MRI Data

Gert Jan Marseille*, Coen van Meijeren*, Iraklis M. Spiliotis, Dirk van Ormondt* and Basil G. Mertzios****

**Department of Applied Physics, Delft University of Technology, The Netherlands, and **Department of Electrical and Computer Engineering, Democritus University of Thrace, Hellas, Greece*

Abstract

A perennial challenge in MRI is reduction of the scan time. An obvious way to achieve this goal is to simply acquire fewer samples in the k-space. This strategy poses a problem to estimation (reconstruction) of the image from the k-space data because the attendant system of equations has become underdetermined. We solve the problem by imposing general prior knowledge in a Bayesian setting.

1 Introduction

This work concerns reduction of the MRI scan time. A full scan usually involves acquisition of 256×256 samples, arranged in a "raw" data matrix $S(k_x, k_y)$. The independent k space variables k_x and k_y are integers in the range $-128, -127, \ldots, +127$. Reduction of scan time can be achieved by omitting a number of k_y-values (rows). The omitted k_y's can be chosen such that the loss of information is minimized [1]. See example in Figure 1. We call data matrices with empty rows, sparse.

If no samples at all are omitted, *i.e.* if the scan is full, mere 2D FFT of $S(k_x, k_y)$ suffices to generate an MR image $I(x, y)$, x and y being integers in the range $-128, -127, \ldots, +127$. However, in the case of sparse sampling such as in Figure 1, the attendant inverse problem is strongly underdetermined. Zero-filling of omitted samples and subsequent application of FFT produces strong artefacts, rendering the image useless. To overcome this problem, one may invoke prior knowledge about the image. However, such prior knowledge ought to be of general nature, so as to avoid bias. In the following, we describe our choice of prior knowledge and its imposition by way of an iterative Bayesian procedure that shuttles back and forth between measurement domain and image domain using FFT and inverse FFT. As already mentioned in the caption of Figure 1, k_x values are *not* omitted because this yields no scan time reduction [2]. Hence, estimation of missing data is not necessary in the k_x-space, and 1D FFT of all rows of $S(k_x, k_y)$ can be tacitly carried out prior to all processing described

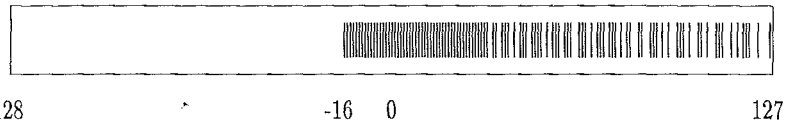

Figure 1. k_y values (bars) of a sparse 2D sample distribution yielding 57% scan time reduction. The positions of the used sample positions k_y is such that the acquired information is maximized [1]. The densely sampled central region $|k_y| \leq n_{\text{central}} = 16$ or 32 is used for estimating a low-resolution version of the image. The omitted samples are estimated with a Bayesian procedure that invokes prior knowledge. Omission of sample positions in the k_x space does not yield scan time reduction and is therefore not done [2]

below. In keeping with this, the data matrix is henceforth written as $S(x, k_y)$, where x is an integer in the range $-128, -127, \ldots, +127$.

2 Prior knowledge of MR images

2.1 Preliminaries

In MR, both the data $S(x, k_y)$ and the image $I(x, y)$ are complex-valued. In absence of noise and phase errors, the real part of the image, $I'(x, y) \stackrel{\text{def}}{=} \text{Re}\, I(x, y)$, is nonnegative within the perimeter of the object O, and zero elsewhere. The imaginary part of the image, $I''(x, y) \stackrel{\text{def}}{=} \text{Im}\, I(x, y)$, is zero everywhere. In actual practice, both $I'(x, y)$ and $I''(x, y)$ contain white Gaussian measurement noise at all coordinates x, y. The 256 × 256 discrete pairs of these coordinates are called *pixels*. In addition, phase errors appear unavoidable and result in mixing of $I'(x, y)$ and $I''(x, y)$. These phase errors need to be estimated and taken into account. The remainder of this section treats the various kinds of prior knowledge used in the Bayesian estimation of the image from sparse (*i.e.*, incomplete) data, including the object perimeter and the phase correction.

2.2 The object prior

An important piece of general information is contained in the probability distribution of *differences* of neighbouring pixel intensities within O: Fuderer found empirically that this distribution possesses Lorentzian (Cauchy) shape [3], and used it to reduce MR image estimation artefacts. This property was applied later by Marseille *et al.* [4, 5], Lettington and Hong [6], and McNally [7]. Defining

$$\delta_y(x, y) \stackrel{\text{def}}{=} I'(x, y) - I'(x, y - 1), \tag{2.1}$$

one can express the probability distribution of the δ's as

$$\mathrm{p}(\delta_y(x,y)) = \frac{1}{a\pi(1+\delta_y(x,y)^2/a^2)}, \tag{2.2}$$

where $(x,y) \in O$, and $2a$ is the width of the distribution at half height. Because no k_x samples were omitted, we do not consider intensity differences in the x direction.

For later use, note that one can write for the case of an image column I'_x comprising for example two separated pieces of object, labeled 1 and 2,

$$\delta_y(x) = \mathbf{D}I'_x, \tag{2.3}$$

where $\delta_y(x)$ is the column vector of all $\delta_y(x,y)$ with common x, and $\mathbf{D}$ is defined by

$$\mathbf{D} = \begin{pmatrix} 0 & \mathbf{D}'(1) & 0 & 0 & 0 \\ 0 & 0 & 0 & \mathbf{D}'(2) & 0 \end{pmatrix}, \quad \mathbf{D}'(.) = \begin{pmatrix} 1 & & & & \\ -1 & 1 & & \mathsf{0} & \\ & \ddots & \ddots & & \\ \mathsf{0} & & -1 & 1 & \\ & & & -1 & 1 \end{pmatrix}. \tag{2.4}$$

In Equation (2.4), 0 and $\mathsf{0}$ represent rectangular and triangular zero matrices of various sizes, respectively.

The size of a can be found by least squares fitting the model of Equation (2.2) to the experimental distribution. However, this distribution is strongly affected by the intentional omission of samples. Rather than fitting the model, our approach is as follows [5]. First we produce an image by zero-filling the omitted samples and applying mere 2D FFT and phase correction. Note that this image is distorted by Gibbs ringing. Next, a is estimated from

$$a = \frac{1}{2}\sqrt{\frac{\sum\limits_{(x,y)\in O} \delta_y(x,y)^2}{N_O - 1}}, \tag{2.5}$$

where N_O is the number of pixels belonging to the object. In words, a is determined by the standard deviation of the intensity differences of the Gibbs ring-distorted image. The size of a is not altered in any stage of the remaining reconstruction process, experiments indicating that such alterations have only marginal effect.

For the sake of simplicity, we assume that the Lorentz distribution applies also to individual columns I'_x of I, and that a is the same for each column.

2.3 The background prior

In the real part of a phase-corrected image, one distinguishes the object O and the background B. Both O and B contain white Gaussian measurement noise

with zero mean and standard deviation σ. Thus the probability distribution for a background pixel can be expressed as

$$\mathrm{p}(I'(x,y)) = \frac{1}{\sigma\sqrt{2\pi}} \exp(-\frac{I'(x,y)^2}{2\sigma^2}), \quad \text{with } (x,y) \in B. \tag{2.6}$$

The imaginary part of a phase-corrected image contains only white Gaussian measurement noise, with zero mean and the same standard deviation σ and can therefore be called background everywhere. Hence, the probability distribution of a pixel at any position in the field of view (FOV) can be expressed as

$$\mathrm{p}(I''(x,y)) = \frac{1}{\sigma\sqrt{2\pi}} \exp(-\frac{I''(x,y)^2}{2\sigma^2}), \quad \text{with } (x,y) \in \mathrm{FOV}. \tag{2.7}$$

2.4 The object perimeter

The perimeter of an object can be estimated from a histogram of pixel intensities [8]. Figure 2 shows an example for a full (*i.e.* 256×256) scan of a slice of a human head. The histogram shows two distinct peaks, the left-hand one originating from the noise, the right-hand one from the object. In the transition region between the two peaks it is difficult to classify the pixel values. One way to classify is to assign all pixel values between zero and the left-most minimum in the transition region as belonging to the noise. In Figure 2 this criterion appears easily applicable. However, for other objects, such as a spine with lungs, the classification can be problematic [5].

As in Section 2.2, an additional complication is that our scans are sparse. In order to avoid hampering the pixel classification by Gibbs ringing, we estimate the object perimeter from only the fully sampled central part of the data matrix $S(x,k_y)$, $|k_y| \leq n_{\mathrm{central}}$ [5, 8], n_{central} usually being 16 or 32. The procedure is as follows.

1. Zero-filling of the samples $k_y > n_{\mathrm{central}}$. This removes ringing due to the irregular sampling shown in the right half of Figure 1.
2. Row-wise weighting of the central samples ($|k_y| \leq n_{\mathrm{central}}$) by a Hanning window. This removes ringing due the fact that the signal has not nearly died out at $|k_y| = n_{\mathrm{central}}$.
3. FFT of each column.

The resulting image has been freed from ringing, but now the resolution is low so that classification of pixels remains problematic.

To cope with these complications, we devised an alternative classification method based on the probability density function for measurement noise in a background pixel of the *magnitude* image $|I(x,y)|$ [9]

$$\mathrm{p}(|I(x,y)|,\sigma) = \frac{|I(x,y)|}{\sigma^2} \exp(\frac{-|I(x,y)|^2}{2\sigma^2}). \tag{2.8}$$

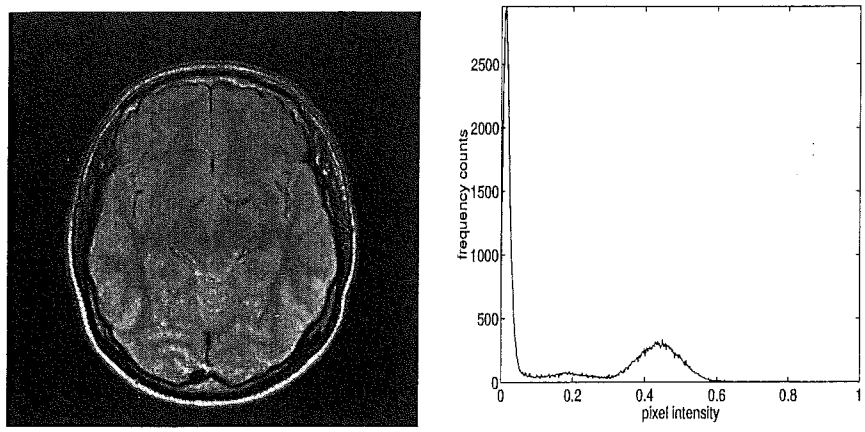

a b

Figure 2. (a) 256 × 256 real-world MR image of an axial slice of a human brain, and (b) histogram of pixel intensities $I'(x, y)$ corresponding to (a). Pixel values are scaled between 0 and 1. Two peaks can be distinguished in (b). The left-hand peak, near zero, originates from the noise in the backgrond; the right-hand peak, around 0.45, originates from the object

Note that the distribution of Equation (2.8) peaks at $|I(x, y)| = \sigma$. Hence, fitting Equation (2.8) to the left-hand peak of the pixel intensity histogram derived from the low-resolution magnitude image, immediately yields σ. Figure 3 shows the result of this fit for the same object as in Figure 2 and $n_{\text{central}} = 32$. Empirically, assigning all pixels with $|I(x, y)| \geq 5\sigma$ to the object appeared a good criterion for automatic perimeter estimation. It turned out that the remaining classification errors have no significant consequences so long as they amount to assigning a background pixel to the object. However, the reverse error, *i.e.* assigning an object pixel to the background, can lead to unacceptable image distortion.

2.5 The phase correction

The phase correction is estimated from the low-resolution image described above, prior to taking the absolute value. The phase of each pixel follows simply from the arctan of the ratio of the real and imaginary parts. A typical result for a slice of a human head scanned with the low phase-distortion "spin-echo" technique [5] is shown in Figure 4. It can be seen that the phase varies smoothly over the low-resolution image. There appeared no need to improve the phase estimate at a later stage in the iterative Bayesian reconstruction in which omitted samples are approaching their true values and need not be zero-filled per se to avoid strong Gibbs ringing. However, when using the high phase-distortion (but faster)

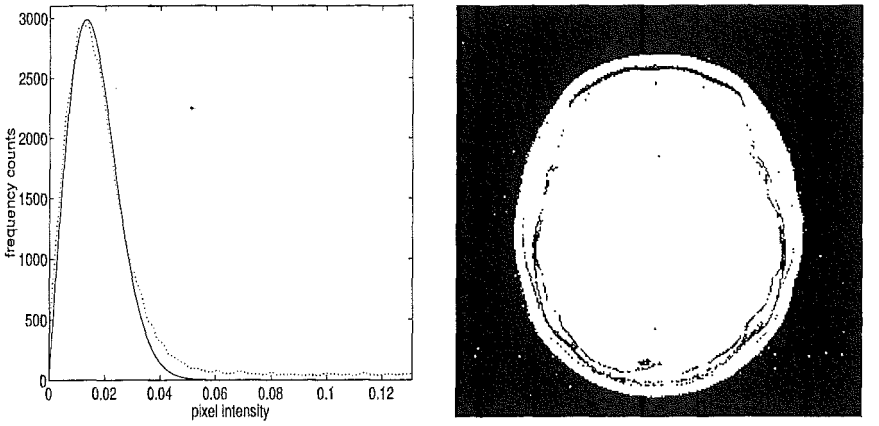

a b

Figure 3. (a) Fit of the model function Equation (2.8) to the noise-peak of the histogram of the low-resolution magnitude image of the object shown in Figure 2(a). The standard deviation of the noise σ is equated to the position of the top of the model function, and (b) resulting object perimeter estimate by setting the threshold at 5σ

"gradient-echo" technique, it appeared advantageous to update the phase after each iteration of the reconstruction procedure.

2.6 The prior knowledge combined

The prior knowledge about pixel intensities and pixel intensity differences will now be combined. We do this for each column I'_x of the phase-corrected image I' separately, ignoring correlation between columns. According to [10], the probability that events $\{A_1, A_2, \ldots, A_n\}$ occur simultaneously can be written as

$$\mathrm{p}(A_1, A_2, \ldots, A_n) = \mathrm{p}(A_1)\,\mathrm{p}(A_2|A_1)\,\mathrm{p}(A_3|A_2, A_1), \ldots, \mathrm{p}(A_n|A_{n-1}, \ldots, A_1). \tag{2.9}$$

If event A_m is independent, then $\mathrm{p}(A_m|A_{m-1}, \ldots, A_1) = \mathrm{p}(A_m)$. However, if event A_m depends on event A_{m-1} but is independent of all others, then $\mathrm{p}(A_m|A_{m-1}, \ldots, A_1) = \mathrm{p}(A_m|A_{m-1})$. Application of these results to the real part of a phase-corrected image column I'_x with elements $\{I'_x(1), I'_x(2), \ldots, I'_x(n)\}$, and comprising for example a single object with perimeters l and m, yields

$$\begin{aligned} \mathrm{p}(I'_x) \;=\; & \mathrm{p}(I'_x(1))\,\mathrm{p}(I'_x(2)) \ldots \mathrm{p}(I'_x(l)) \times \\ & \mathrm{p}(I'_x(l+1)|I'_x(l))\,\mathrm{p}(I'_x(l+2)|I'_x(l+1)) \ldots \mathrm{p}(I'_x(m-1)|I'_x(m-2)) \times \\ & \mathrm{p}(I'_x(m))\,\mathrm{p}(I'_x(m+1)) \ldots \mathrm{p}(I'_x(n)). \end{aligned} \tag{2.10}$$

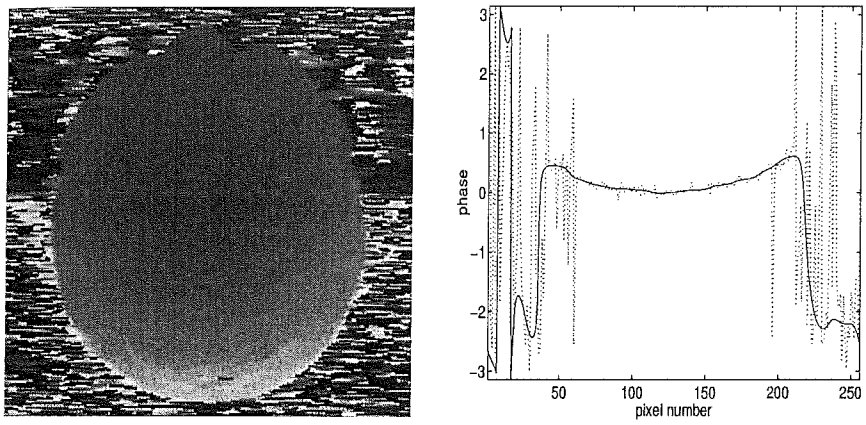

a b

Figure 4. (a) Low-resolution ($n_{\text{central}} = 32$) phase estimate (proportional to grey value) of a slice of a human brain scanned with the "spin-echo" technique. Within the object, the phase varies gradually between $-\pi$ (black) and π (white), and (b) phase (in radians) of one image row. The dotted and solid line are the phase of the full-resolution image and low-resolution image respectively

Noting that terms of the form $\mathrm{p}(I'_x(l+r)|I'_x(l+r-1))$ are governed by the Lorentzian probability distribution treated in Section 2.2, one can finally write

$$\begin{aligned} \mathrm{p}(I_x) &= \frac{1}{(\sigma\sqrt{2\pi})^{b_x}} \exp[-\frac{1}{2\sigma^2} \sum_{y \notin O_x} I'(x,y)^2] \\ &\times \frac{1}{(\sigma\sqrt{2\pi})^{n}} \exp[-\frac{1}{2\sigma^2} \sum_{\forall y} I''(x,y)^2] \\ &\times \prod_{y \in O_x} \frac{1}{a\pi(1+\delta_y(x,y)^2/a^2)} \end{aligned} \tag{2.11}$$

with $x = -128, -127, \ldots, 127$, b_x is the number of background pixels (*i.e.*, outside O_x), $n = 256$.

We mention that additional knowledge is often available when measuring a series of MR scans of an object that varies with time. This pertains to the fact that each scan of the series can benefit from information gained from previous scans [11]. The latter is beyond the scope of this contribution.

3 Bayesian image reconstruction

3.1 Strategy for underdetermined systems

Bayesian estimation lends itself well to accommodation of prior knowledge [12, 13, 14]. For the present problem, the well-known Bayes formula can be written as

$$\mathrm{p}(I_x|S_x) = \frac{\mathrm{p}(S_x|I_x)\,\mathrm{p}(I_x)}{\mathrm{p}(S_x)}, \tag{3.1}$$

in which I_x is a column of the image I and S_x is the related column of the sparse raw data matrix $S(x, k_y)$. Furthermore, the posterior $\mathrm{p}(I_x|S_x)$ is the probability density function of I_x after collecting the data, the likelihood $\mathrm{p}(S_x|I_x)$ is the probability density function of the noise superimposed on the data, the prior knowledge $\mathrm{p}(I_x)$ has been treated above, and the evidence $\mathrm{p}(S_x)$ is just a scaling factor. The task is to find for each x the image column I_x that maximizes the posterior $\mathrm{p}(I_x|S_x)$. In the standard Bayesian procedure, the resulting image is a trade-off between the measured data and the invoked prior knowledge. The present approach differs from this in the following sense. Since S_x is sparse, our system is underdetermined. We maximize the posterior by adjusting the omitted samples subject to the available prior knowledge and leaving the measured samples untouched. Note that not touching the data amounts to treating them as ideal which in turn implies that the likelihood $\mathrm{p}(S_x|I_x)$ becomes a constant factor.

3.2 Maximization of the posterior

Maximizing the posterior is equivalent to minimizing minus its natural logarithm. Dropping constant terms, the natural logarithm of the posterior becomes

$$\begin{aligned} &\ell_x \stackrel{\text{def}}{=} -\ln \mathrm{p}(I_x|S_x) \Longrightarrow \\ &\tfrac{1}{2\sigma^2} I_x'^{\mathrm{T}} \mathbf{B} I_x' + \sum_{y \in O} \ln[1 + \delta(y)^2/a^2] + \tfrac{1}{2\sigma^2} I_x''^{\mathrm{T}} I_x'', \end{aligned} \tag{3.2}$$

where $\mathbf{B}$ is an n × n diagonal matrix with diagonal entries

$$\mathbf{B}(y,y) = \begin{cases} 1 & \text{if } I_x(y) \notin O_x, \\ 0 & \text{if } I_x(y) \in O_x. \end{cases} \tag{3.3}$$

The quantity ℓ_x defined in Equation (3.2) is to be minimized as a function of the omitted samples, subject to the conditions

$$\begin{aligned} &1)\ I_x = \mathbf{W}^{-1} S_x, \\ &2)\ \text{measured data remain unchanged,} \end{aligned} \tag{3.4}$$

where $\mathbf{W}$ is the DFT matrix

$$\mathbf{W}(u,v) = w^{uv} \quad \text{with} \quad \begin{cases} w = \exp(2\pi i/n), \\ u = -n/2, \ldots, n/2 - 1, \\ v = -n/2, \ldots, n/2 - 1. \end{cases} \tag{3.5}$$

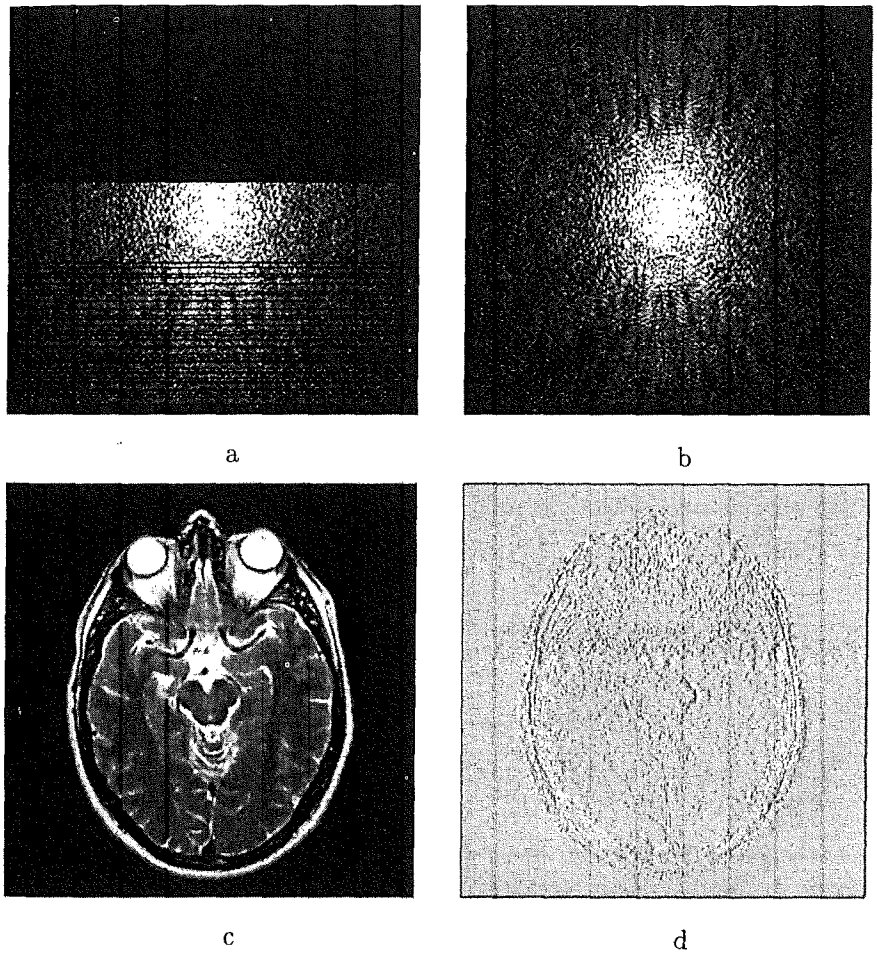

Figure 5. Spin-echo scan time reduction by 57% for a slice of a human head by sparse sampling. (a) Magnitude of the sparse data matrix, $|S(k_x, k_y)|$, on a logarithmic scale. The black rectangle and black lines represent omitted data, (b) same as (a), but now the omitted samples have been estimated with the iterative Bayesian procedure described in this paper, (c) 2D FFT of the phase-corrected reconstructed data matrix $S(k_x, k_y)$, and (d) difference between (c) and the 2D FFT of the full scan

Although ℓ_x is not convex we found empirically that a gradient search for its minimum does not critically depend on the choice of starting values of the omitted samples [5]. Hence, starting with zeros is adequate. For minimization, we use the iterative conjugate gradients method [15]. The search direction, $\mathrm{d}S_x^{(j)}$, in iteration j is given by

$$\mathrm{d}S_x^{(j)} = -\nabla \ell_x(S_x^{(j)}) + \frac{\|\nabla \ell_x(S_x^{(j)})\|^2}{\|\nabla \ell_x(S_x^{(j-1)})\|^2}\,\mathrm{d}S_x^{(j-1)}. \tag{3.6}$$

The columns S_x comprise measured data and omitted data. As mentioned earlier, the former are left untouched whereas the latter are updated in each iteration. The gradient of ℓ_x with respect to the omitted data is [5]

$$\nabla \ell_x(S_x) = \mathbf{MW}(\frac{\partial \ell_x}{\partial I_x})^{\mathrm{T}}, \tag{3.7}$$

in which $\mathbf{M}$ is a diagonal matrix with diagonal entries

$$\mathbf{M}(k_y, k_y) = \begin{cases} 0 & \text{if } S_x(k_y) \text{ has been measured,} \\ 1 & \text{if } S_x(k_y) \text{ has been omitted,} \end{cases} \tag{3.8}$$

and

$$\frac{\partial \ell_x}{\partial I_x} = \frac{\partial \ell_x}{\partial I_x'} + i\frac{\partial \ell_x}{\partial I_x''} \tag{3.9}$$

$$\frac{\partial \ell_x}{\partial I_x'} = \frac{\partial \ell_x}{\partial I_x'} + \frac{\partial \ell_x}{\partial \delta_y(x)}\frac{\partial \delta_y(x)}{\partial I_x'} = (\frac{1}{\sigma^2}\mathbf{B}I_x' + \mathbf{D}^{\mathrm{T}}(\frac{\partial \ell_x}{\partial \delta_y(x)})^{\mathrm{T}})^{\mathrm{T}} \tag{3.10}$$

$$\frac{\partial \ell_x}{\partial I_x''} = (\frac{1}{\sigma^2}I_x'')^{\mathrm{T}} \tag{3.11}$$

$$\frac{\partial \ell_x}{\partial \delta_y(x,y)} = \frac{2\delta_y(x,y)}{a^2 + \delta_y(x,y)^2}, \tag{3.12}$$

where $i = \sqrt{-1}$. Finally, the linear search parameter λ_j of the omitted data update in iteration j is the smallest possible positive number that minimizes $\ell_x(S_x^{(j)} + \lambda_j \mathrm{d}S_x^{(j)})$ [5]. The iterations are pursued until the changes of the omitted samples become insignificant. Note that in each iteration the agreement between the inverse FFT of the image and the measured samples is exact.

Summarizing, the iterative Bayesian image estimation from sparse raw data runs as follows.

1. FFT in k_x space of measured rows of $S(k_x, k_y)$, resulting in $S(x, k_y)$.
2. Zero-filling of omitted rows of $S(x, k_y)$.
3. Estimation of a starting image by FFT in k_y space.
4. Estimation of a low-resolution image from the fully sampled region $|k_y| \leq n_{\text{central}}$ (see Figure 1), n_{central} =16 or 32, $-128 \leq k_x \leq +127$.

5. Estimation of the object perimeter and phase error map from the low-resolution image, to be used as *prior knowledge.*
6. Correction of phase errors in the current image.
7. Computation of an image update from prior knowledge. This can be done for each column separately.
8. Undoing of the phase correction.
9. Conversion of the image update to the k_y space by IFFT. Measured data are left intact.
10. If the changes of omitted samples are sufficiently small, then the current image becomes the final image. Else, go to 6 preceded by a better phase error estimate in the case of gradient-echo scanning.

Reconstruction (estimation) of an image column from real-world raw data usually converges in ten to fifteen iterations. Using a SUN SPARCstation 5 and Fortran77, this takes 0.2 seconds. For a complete image, this is to be repeated for up to 256 columns. Figure 5 shows a successful application to a spin-echo scan of a slice of a human head yielding 57% scan time reduction. With gradient echoes, the scan time reduction is less because of the phase errors incurred.

4 Conclusions

- Sparse irregular sampling combined with Baysian image estimation and prior knowledge yields substantial scan time reduction.
- Additonal prior knowledge is sought, especially for "dynamic" scans.
- The computation time is presently too long for on-line use.

Acknowledgment

This work is supported by the EU programme HCM/Networks, the Dutch Research Foundation STW, Philips Medical Systems, and the Advanced School for Computing and Imaging (ASCI).

Bibliography

1. Marseille, G.J., Beer, R. de, Fuderer, M., Mehlkopf, A.F., Ormondt, D. van (1996), Nonuniform Phase-Encode Distributions for MRI Scan Time Reduction, *J. Magn. Reson. B*, **111**, 70-75.
2. Liang, Z.P., Boada, F.E., Constable, R.T., Haacke, E.M., Lauterbur, P.C, Smith, M.R. (1992), Constrained Reconstruction Methods in MR Imaging, *Reviews of Magnetic Resonance in Medicine*, **4**, 67-185.

3. Fuderer, M. (1989), Ringing Artefact Reduction by an Efficient Likelihood Improvement Method, *Proc. SPIE*, **1137**, 84-90.

4. Marseille, G.J., Fuderer, M., Beer, R. de, Mehlkopf, A.F., and Ormondt, D. van (1994), Reduction of MRI scan time through nonuniform sampling and edge-distribution modeling, *J. Magn. Reson. B*, **103**, 292-295.

5. Marseille (1997), MRI scan time reduction through nonuniform sampling, *Ph D Thesis*, Delft University of Technology.
http://dutnsic.tn.tudelft.nl:8080/main/main.html

6. Lettington, A.H. and Quong, Q.H. (1995), Image restoration using a Lorentzian probability model, *J. Modern Optics* , **42**, 1367-1376.

7. McNally, B. (1996), Lorentzian Probability Model, *Internal Report*, King's College London, London, UK, 16-17.

8. Spiliotis, I.M., Ormondt, D. van, Mertzios, B.G. (1995), Prior Knowledge for Improved Image estimation from Raw MRI Data, *Conf. Proc. 2nd International Workshop on Image and Signal Processing: Theory, Methodology and Applications*, Budapest, Hungary, 8-10 November 1995, 274-283.

9. Bernstein, M.A., Thomasson, D.M., and Perman, H. (1989), Improved detectability in low signal-to-noise ratio magnetic resonance images by means of a phase-corrected real reconstruction, *Med. Physics* **16** (5), 813-817.

10. Blum, J.R., Rosenblatt, J.I. (1972), Probability and Statistics, Saunders, Philadelphia.

11. Chandra, S., Liang, Z.P., Webb, A., Lee, H., Morris, H.D., Lauterbur, P.C. (1996), Application of Reduced-Encoding Imaging with Generalized-Series Reconstruction (RIGR) in Dynamic MR Imaging, *JMRI*, **6**, 783-797.

12. Norton, J.P. (1986), An Introduction to Identification, Academic Press, London.

13. Gelman, A., Carlin, J.B., Stern, H.S., Rubin, D.B. (1996), Bayesian Data Analysis, Chapman & Hall, London.

14. Sivia, D.S. (1996), Data Analysis. A Bayesian Tutorial, Clarendon, Oxford.

15. Fletcher, R., Reeves, C.M. (1964), Function minimization by conjugate gradients, *The Comp. J.* **7**, 149-154.